ACS OMEGA

Open Access

http://pubs.acs.org/journal/acsodf

Article

Electrospun Carvacrol-Loaded Polyacrylonitrile/Poly(ethylene oxide) Nanofibrous Films as Wound Dressings

Shuo Wang, Xinyuan Xu, Xiangyu Zhu, Xiao Tan, and Bei Xie*

Cite This: *ACS Omega* 2024, 9, 39472−39483

Read Online

ACCESS | Metrics & More | Article Recommendations

ABSTRACT: Preventing microbial infections and accelerating wound closure are essential in the process of wound healing. In this study, various concentrations of carvacrol (CA) were loaded into polyacrylonitrile/poly(ethylene oxide) (PAN/PEO) nanofiber membranes to develop potential wound dressing materials via an electrospinning technique. The morphology and structure of the PAN/PEO/CA nanofiber membrane were analyzed by scanning electron microscopy (SEM) and Fourier transform infrared spectroscopy (FTIR), respectively. Subsequently, antimicrobial performance testing showed that the PAN/PEO/CA nanofiber membrane exhibited antimicrobial activity in a concentration-dependent manner. Moreover, SEM and transmission electron microscopy revealed that the number of *Staphylococcus aureus* decreased significantly and the microstructure of the biofilm was seriously damaged. Next, compared with the control and PAN/PEO groups, the PAN/PEO/5% CA group in a full-thickness skin infection model not only exhibited reduced wound exudate on day 2 after infection but also displayed a greater ability to achieve complete skin regeneration, with faster wound healing. Finally, the Kyoto Encyclopedia of Genes and Genomes pathway analysis revealed that the downregulated differentially expressed genes between PAN/PEO- and PAN/PEO/5% CA-treated *S. aureus* were enriched in the two-component system and *S. aureus* infection. In conclusion, the antimicrobial materials of PAN/PEO/CA inhibited microbial growth and promoted wound healing with potential applications in the clinical management of wounds.

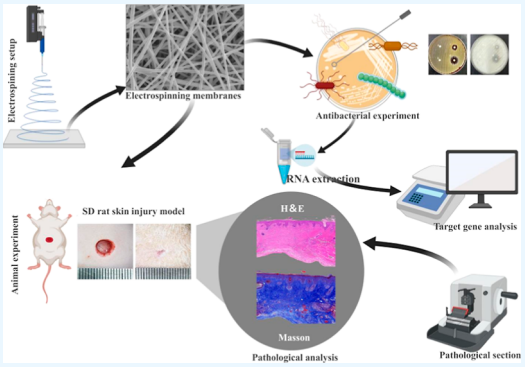

1. INTRODUCTION

Clinically, the skin exposed following an injury is susceptible to numerous unknown or challenging microbial infections.[1−3] Wound treatment can be expensive, and most available wound dressings have limitations such as poor antimicrobial activity, toxicity, inability to absorb wound exudate, and inferior mechanical performance.[4] Ideal wound dressings should have both healing properties and characteristics, such as absorbency of wound exudate, appropriate breathability, controlled release of medications, and a certain level of mechanical strength and porosity to ease cell attachment, migration, and proliferation.[5,6]

Electrospinning is a cutting-edge technology that enables the creation of a wide range of nanofibers. By applying an electric field and utilizing intermolecular interactions within high-viscosity spinning solutions, polymer solutions can be elongated to form continuous and tightly packed nanofibers.[7] Electrospinning produces a porous interconnected network of nanofibers. Mesh-like porous structures aid in the absorption of wound exudate, favor gaseous exchange, and provide support for cell infiltration and proliferation, good tissue compatibility, and exceptional mechanical properties.[8−10] Electrospinning is moving from single-fluid electrospinning to coaxial electrospinning, side-by-side electrospinning, and multiple-fluid electrospinning for producing complicated structures and encapsulating more kinds of active ingredients.[11−16] However, the single-fluid blending process remains mainstream in this field and can avoid the complexity of multiple-fluid processes for robust preparation and potential industrial applications.

Electrospinning nanofibers are highly flexible materials that are used as carriers for therapeutic dressings to accelerate wound healing while reducing inflammation.[17] In addition, nanofibers of different polymers simulate the structure of the extracellular matrix and provide the best biomimetic physiological environment for cell and tissue regeneration, thereby making them ideal wound repair material. Several practical examples have already demonstrated their effectiveness in preventing wound bacterial colonization and infection while creating an optimal environment for healing. For example, composite nanofibers with poly(vinyl alcohol)

Received: April 8, 2024
Revised: August 17, 2024
Accepted: September 2, 2024
Published: September 13, 2024

(PVA) and chitosan were developed for the purpose of dual drug therapy in wound treatment.[18] POSS-reinforced chitosan-based bilayer sponges loaded with *Cissus quadrangularis* were prepared for wound healing applications.[19] Therefore, electrospinning nanofibers loaded with antibacterial agents have emerged as a promising therapeutic option. An ideal polymer for wound dressings should possess properties such as biodegradability, bacterial impermeability, and the ability to maintain moisture content over the wound surface. Polyacrylonitrile (PAN) possesses outstanding mechanical properties and chemical stability. It can be easily synthesized into nanofibers by electrospinning and used as a drug delivery carrier.[10,20,21] However, it is unsuitable as a hydrophobic polymer for preventing fluid removal from the wound surface. To overcome this problem, which comes from its hydrophobic nature, PAN can be used in combination with water-soluble poly(ethylene oxide) (PEO). Hydrophilic PEOs are often mixed with other polymeric materials to produce composite nanofibers.[22,23] PEO could improve the wettability and swelling of blended fibers of PEO and PAN. The degree of swelling impacts the effectiveness of a particular system in removing wound exudate, which would enhance the process of wound repair.[24] In addition, a greater proportion of cells adhered to the altered hydrophilic surface of the electrospinning mats, resulting in an improved environment for cell proliferation.[25] Carvacrol (CA) is a monoterpenoid phenolic compound extracted from plants, and it possesses biological and pharmacological characteristics, such as small molecular size, low polarity, low toxicity, and exhibits different active properties, including antimicrobial, antioxidant, anticancer, and anti-inflammatory effects.[26,27] The hydrophobic and volatile nature of CA poses a challenge when it is used as an encapsulated drug for tissue engineering. Therefore, various carriers were invented to overcome volatility and prolong the effectiveness of CA.

Plant extracts can be effectively encapsulated into electrospun nanofibers, and their thermal stability, controlled release, and shelf life can be enhanced and extended due to the characteristics of polymer nanofibers.[28−30] In this study, we successfully fabricated nanofibers using electrospinning technology by utilizing a blended solution of PAN and PEO. The novel integration of PAN and PEO composite fibers infused with CA was initially utilized to improve the antimicrobial performance and repair of damaged skin. To evaluate the physical and biological properties of the nanofiber membranes, we first characterized the PAN/PEO and PAN/PEO/CA membranes via scanning electron microscopy (SEM), Fourier transform infrared (FTIR) spectroscopy, and contact angle. Then, the antimicrobial ability of the membranes was studied by using Gram-positive bacteria, Gram-negative bacteria, and fungi. Finally, the ability to repair wounds was verified through an in vivo model of *Staphylococcus aureus* infection.

2. EXPERIMENTAL SECTION

2.1. Materials. PAN (Changsha Nanoapparatus Co., Ltd., molecular weight, 150,000), PEO (Dongguan Zhanyang Polymer Materials Co., Ltd., molecular weight 10,000), *N*,*N*-dimethylformamide (DMF; 99%, biotechnology grade, Shanghai Macklin Biochemical Technology Co., Ltd.), CA ($C_{10}H_{14}O$, 99%, Shanghai Aladdin Biochemical Technology Co., Ltd.), yeast extract (OXOID LP0021), tryptone (Sangon Biotech), agar (Sangon Biotech), NaCl (Sangon Biotech), electron microscope fixing solution (Servicebio), *S. typhimurium* (ATCC 14028), *B. subtilis* (ATCC 6633), *S. aureus* (ATCC 6538), *E. coli* (ATCC 25922), *Cissus albicans* (ATCC 10231), and *A. fumigatus* (AF293) were obtained from the Key Laboratory of Molecular Biology of Shaoyang University. The agar plate was prepared as follows: NaCl (2 g), tryptone (2 g), yeast extract (1 g), and agar (4 g) were added to 200 mL of ultrapure water to obtain liquid culture medium. After sterilization, they were poured into culture dishes and cooled to obtain agar culture plates.

2.2. Preparation of the PAN/PEO/CA Composite Nanofiber Membranes. *2.2.1. Preparation of the Spinning Solution.* 2 g of PAN and 1 g of PEO were added into 20 mL of DMF solvent and mixed to obtain PAN/PEO electrospinning solution. The mixture was thoroughly stirred using a heated magnetic stirrer at room temperature for 12 h. Afterward, CA was added separately to the PAN/PEO mixed solution to achieve concentrations of 5% CA (w/v) and 10% CA (w/v). The resulting mixture was placed back into the magnetic stirrer until it was completely dissolved.

2.2.2. Preparation of the Composite Nanofiber Membranes. 15 mL portion of the prepared spinning solution was placed into the electrospinning machine (Changsha Nanoapparatus Co., Ltd.) for spinning. The spinning flow rate was 1 mL/h, spinning voltage was 15.04 kV, and spinning back-and-forth distance was 50 mm. After spinning, the PAN/PEO, PAN/PEO/5% CA, and PAN/PEO/10% CA composite nanofiber membranes were obtained. The composite nanofiber membranes were sliced into small round pieces with a consistent thickness of 5 mm in diameter. Next, the membranes were placed in a laminated bag and stored in an ultraclean workbench for UV sterilization for 60 min.

2.3. Fiber Characterization and Detection. *2.3.1. Fiber Morphology Test.* The nanofiber membranes were coated by using a Cressington 208HR high-resolution sputter coater at 20 mA for 120 s, followed by SEM testing (Thermo Scientific Apreo 2C).

2.3.2. FTIR Spectroscopy. The nanofiber membranes were crushed and mixed with potassium bromide powder, followed by grinding to ensure uniformity. The resulting mixture was pressed into pellets, and its chemical structure was detected by using FTIR (Germany Bruker Optic GmbH).

2.3.3. Contact Angle Detection. The static contact angle was measured by using the sessile drop method. The samples were placed on a test stage and adjusted to obtain a clear view and focus. Next, 3 μL of the test liquid was vertically dropped onto the sample surface. After the images were focused, an image was acquired to determine the contact angle (OCA 20, Germany DataPhysics).

2.4. Antimicrobial Properties. *2.4.1. Diffusion Test.* The People's Republic of China GBT 20944.1−2007 "Evaluation Standard for Antimicrobial Performance of Textiles (Agar Plate Diffusion Method) was followed to characterize the antimicrobial activity of nanofiber surfaces by observing the size of the inhibition zone. Different nanofiber membranes (PAN/PEO, PAN/PEO/5% CA, and PAN/PEO/10% CA) were cut into small circular discs with a diameter of 5 mm. These fibers were attached to agar plates coated with different microorganisms after being sterilized with ultraviolet radiation. The size of the antimicrobial zone increased after 24 h.

2.4.2. Oscillation Test. Microbial suspension was obtained by dipping a certain amount of microbes in the inoculation ring and then dispersing the microbe in the liquid medium. The OD values of the different microbial suspensions at 560

https://doi.org/10.1021/acsomega.4c03140
ACS Omega 2024, 9, 39472−39483

nm were as follows: *S. aureus* (OD = 0.080), *E. coli* (OD = 0.123), *S. typhimurium* (OD = 0.270), *B. subtilis* (OD = 0.250), *C. albicans* (OD = 0.069), and *A. fumigatus* (OD = 0.270). For each microbial suspension, three different centrifuge tubes were prepared and 1 mL of suspension was placed into each tube. Three different types of membranes (PAN/PEO, PAN/PEO/5% CA, and PAN/PEO/10% CA) were added to each of the three centrifuge tubes, and the tubes were placed in a constant-temperature incubator at 37 °C with a rotation speed of 220 rpm. After agitation for 24 h, 100 μL of the solution from each of the three tubes was streaked on three different nutrient agar plates. The plates were placed in a constant-temperature incubator at 37 °C for 24 h, after which the number of microbial colonies was counted.

2.4.3. Microbial Morphology Observation. Next, the effects of nanofiber membranes on the morphology and ultrastructure of *S. aureus* were studied using SEM and transmission electron microscopy (TEM). Different nanofiber membranes (PAN/PEO, PAN/PEO/5% CA, and PAN/PEO/10% CA) were placed into three 1 mL *S. aureus* suspensions, and then were cultured in a constant-temperature incubator at 37 °C and 220 rpm for 24 h with constant shaking. Afterward, tweezers were used to extract the three composite nanofiber membranes, which were then centrifuged at 8000 rpm for 1 min under these conditions, after which the supernatant was discarded. The precipitate was fixed using an electron microscope fixing solution at room temperature for 2 h, followed by SEM and TEM testing.

2.5. Quantitative Real-Time PCR. Total RNA was extracted using the TRIzol (Invitrogen) method according to the manufacturer's instructions. RNA concentrations were measured using a Nanodrop spectrophotometer (Thermo Scientific). Reverse transcription was performed to produce cDNA using the PrimeScript RT Reagent Kit with a gDNA Eraser (Perfect Real Time) (Takara). RT-PCR analysis was performed using SYBR Green (Vazyme Biotech), and primer sequences of target genes and housekeeping gene are listed in Table 1. Relative gene expression fold changes were identified using the $2^{-\Delta\Delta Ct}$ method after normalization to the housekeeping gene.

Table 1. Sequences of Primers Used for RT-PCR

primer name	primer sequence (5′ → 3′)
icaA-F	GATACTGATATGATTACCGAAGAT
icaA-R	GAACCAACATCCAACACAT
agrA-F	TGAAATTCGTAAGCATGACCC
agrA-R	CATCGCTGCAACTTTGTAGAC
sarA-F	TGTTTGCTTCAGTGATTCGTTTA
sarA-R	AACCACAAGTTGTTAAAGCAGTTA
16s RNA-F	CGTGCTACAATGGACAATACAAA
16s RNA-R	ATCTACGATTACTAGCGATTCCA

2.6. Animal Experiments. The Ethics Committee of Shaoyang University approved all animal experiments. Sprague−Dawley (SD) rats weighing 220 g were used to establish an *S. aureus* infection model to study the wound healing process in vivo. All rats were anesthetized with sodium pentobarbital at a concentration of 60 to 70 mg/kg. The hairs on the backs of the rats were shaved, and a diameter of 5 mm was created. Next, a syringe was used to extract the bacterial suspension of *S. aureus,* and then 20 μL was injected into each rat wound. According to the different treatment methods used, the experimental groups were divided into three groups: the control group (with sterile medical transparent dressings), 1 cm diameter PAN/PEO nanofiber membranes, and PAN/PEO/5% CA nanofiber membranes.

After 2 days, the nanofiber membranes were removed, and changes in wound areas were measured at 2, 4, 6, 8, and 10 days. On day 10 postinfection, tissue samples from the wound sites were collected for hematoxylin and eosin (H&E) staining and Masson's trichrome staining to evaluate skin repair. The wound dimension was measured using ImageJ software, and the percentage of wound closure was calculated using the following equation:

Wound healing rate = [(original wound area − unhealed wound area)/original wound area] × 100%.

2.7. RNA Sequencing and Data Analyses. We prepared and cultured 200 mL of *S. aureus* suspensions by oscillation for 5 h to reach the logarithmic growth stage. The PAN/PEO nanofiber membrane was added as the control group, and the PAN/PEO/5% CA nanofiber membrane was added as the treatment group. Each group of samples was repeated three times and centrifuged after oscillation for 19 h. Finally, the supernatant was removed, frozen in liquid nitrogen for 20 min, frozen in an ultralow temperature freezer at −80 °C, and finally sent to Gene Pioneer Biotechnologies (Nanjing, China) for RNA sequencing. Differential expression analysis of samples was conducted using DESeq2 software to screen differentially expressed genes (DEGs). The screening criteria were $|\log_2(\text{fold change})| \geq 1$ and false discovery rate (FDR) < 0.05.

The statistical significance of DEGs and differences between the PAN/PEO and PAN/PEO/5% CA nanofiber membranes were studied using volcano plots. A heatmap was utilized to cluster genes based on their similar or identical expression patterns following the hierarchical cluster analysis of selected DEGs. The gene ontology (GO) terms were categorized into three subgroups: biological process (BP), cellular component (CC), and molecular function (MF). Additionally, the significantly enriched pathways were identified by using the Kyoto Encyclopedia of Genes and Genomes (KEGG) database. Cytoscape plugins were utilized to analyze the interactive relationships among the top 10 hub DEGs.

2.8. Statistical Analysis. The results are presented as the mean ± standard deviation. The significant differences between the two groups were evaluated by using the *t*-test. A *p*-value less than 0.05 was considered significant (*).

3. RESULTS AND ANALYSIS

3.1. Characterization of the Nanofiber Membrane. The morphological characteristics of the PAN, PAN/PEO, PAN/PEO/5% CA, and PAN/PEO/10% CA nanofiber membranes were examined. SEM micrographs of electrospinning nanofibers demonstrated that these nanofibers were randomly aligned throughout the scaffolds. All nanofibers exhibited continuous, porous, and bead-free morphologies (Figure 1). We fabricated CA-incorporated nanofibers and demonstrated that CA integration did not change the orientation or morphology of the nanofibers, and these nanofibers maintained a porous structure. We randomly selected 50 nanofibers for statistical analysis of diameter and found that the average fiber diameter of the pure PAN nanofiber membrane was 0.21 ± 0.05 μm, that of the PAN/PEO membrane was 0.29 ± 0.06 μm, and that of the PAN/PEO/5% CA membrane was 0.38 ± 0.07 μm, whereas the average fiber diameter of the PAN/PEO/10% CA membrane

https://doi.org/10.1021/acsomega.4c03140
ACS Omega 2024, 9, 39472−39483

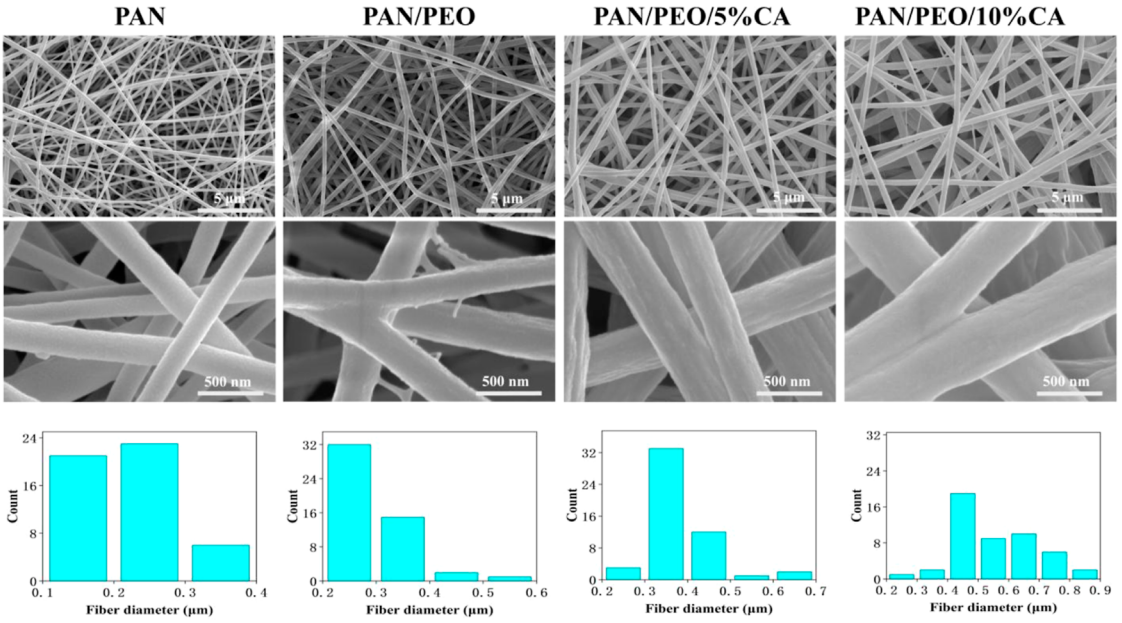

Figure 1. SEM images of the PAN, PAN/PEO, PAN/PEO/5% CA, and PAN/PEO/10% CA nanofiber membranes.

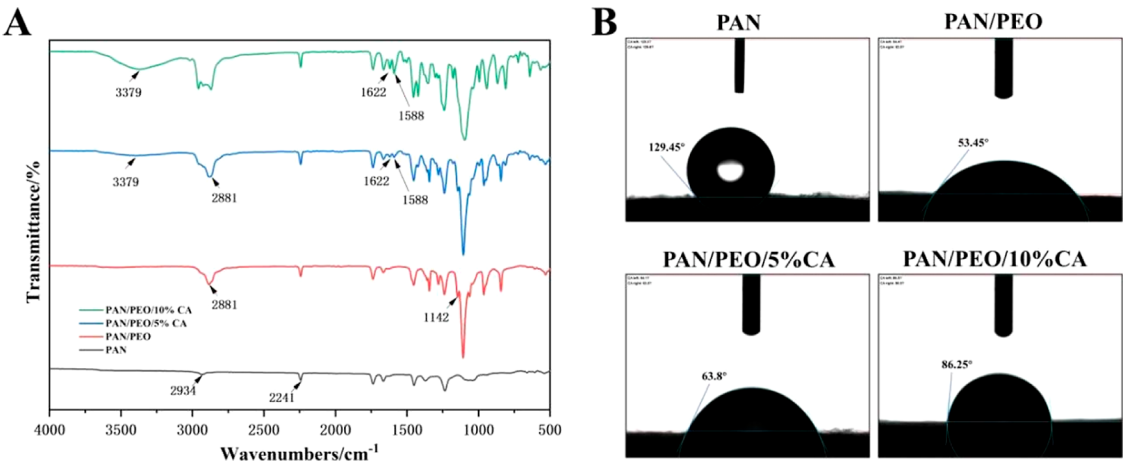

Figure 2. Characterization of PAN, PAN/PEO, PAN/PEO/5% CA, and PAN/PEO/10% CA. (A) FTIR analysis. (B) Contact angle testing.

was 0.54 ± 0.15 μm. After adding PEO and CA, the diameter of the nanofibers became thicker and the surface became rougher. The diameter of the fibers became larger with increasing CA concentration. SEM micrographs demonstrated that CA had an incremental effect on the fiber diameter.

3.2. FTIR Analysis and Contact Angle Analysis. Figure 2A displays the FTIR analysis results for the electrospinning nanofiber membranes composed of PAN, PAN/PEO, PAN/PEO/5% CA, and PAN/PEO/10% CA. The characteristic absorption peak of PAN can be observed from the following curves: the stretching vibration peak of C≡N at 2241 cm^{-1} and the bending vibration peak of $-CH_2-$ at 2934 cm^{-1}.[31] The C−O−C stretching vibration peak and $-CH_2$ stretching vibration peak of PEO can be found in the composite fibers of PAN/PEO, located at 1142 and 2881 cm^{-1}, respectively.[24] PAN/PEO/5% CA and PAN/PEO/10% CA exhibit characteristic functional group infrared absorption peaks with the addition of 10% CA resulting in more significant infrared results. The characteristic peaks located at 1622 and 1588 cm^{-1} belong to the C═C skeleton vibration peak on the benzene ring. The broad peak at 3379 cm^{-1} is attributed to the stretching vibration of −OH.[32] These results indicate that CA was successfully loaded into the PAN/PEO nanofiber membrane.

At a contact angle of θ < 90 deg, the solid surface exhibits hydrophilicity, and liquids were more susceptible to wetting the solid. At θ > 90 deg, the solid surface exhibits hydrophobicity. Figure 2B shows that different nanofiber membranes were subjected to contact angle experiments. Pure PAN nanofibers demonstrated strong hydrophobicity when the average contact angle was 129.45°. The addition of the hydrophilic material PEO significantly improved the hydrophilicity of the mixed nanofiber membrane when the average contact angle was 53.45° for the PAN/PEO nanofibers, which was particularly important for materials used as dressings to adsorb exudate.[24] The contact angles of PAN/PEO/5% CA and PAN/PEO/10% CA were 63.8 and 86.25°, respectively. The contact angle of PAN/PEO/CA was larger than that of PAN/PEO, which may be because CA is a lipid-soluble drug. Compared with PAN/PEO, PAN/PEO/CA exhibited decreased hydrophilicity, and its hydrophilicity decreased with the addition of CA in a concentration-dependent manner.

https://doi.org/10.1021/acsomega.4c03140
ACS Omega 2024, 9, 39472−39483

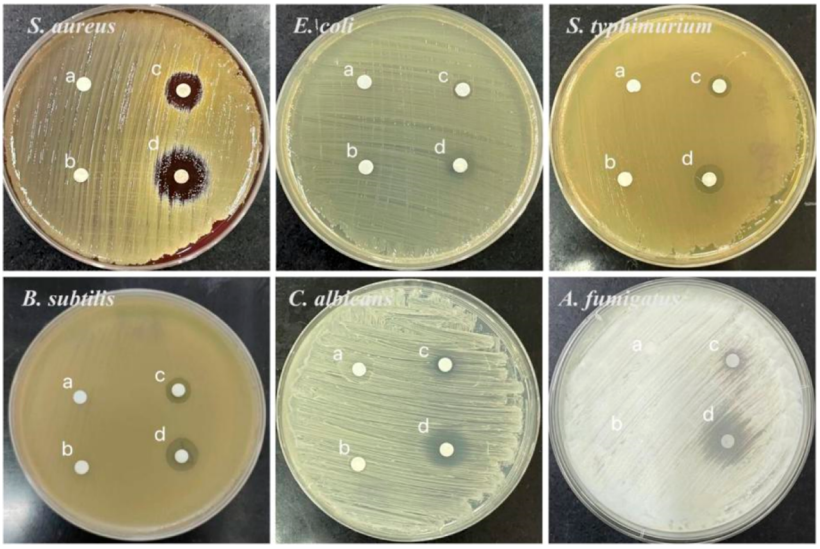

Figure 3. Antimicrobial effects of different nanofiber membranes [(a) pure PAN, (b) PAN/PEO, (c) PAN/PEO/5% CA, and (d) PAN/PEO/10% CA].

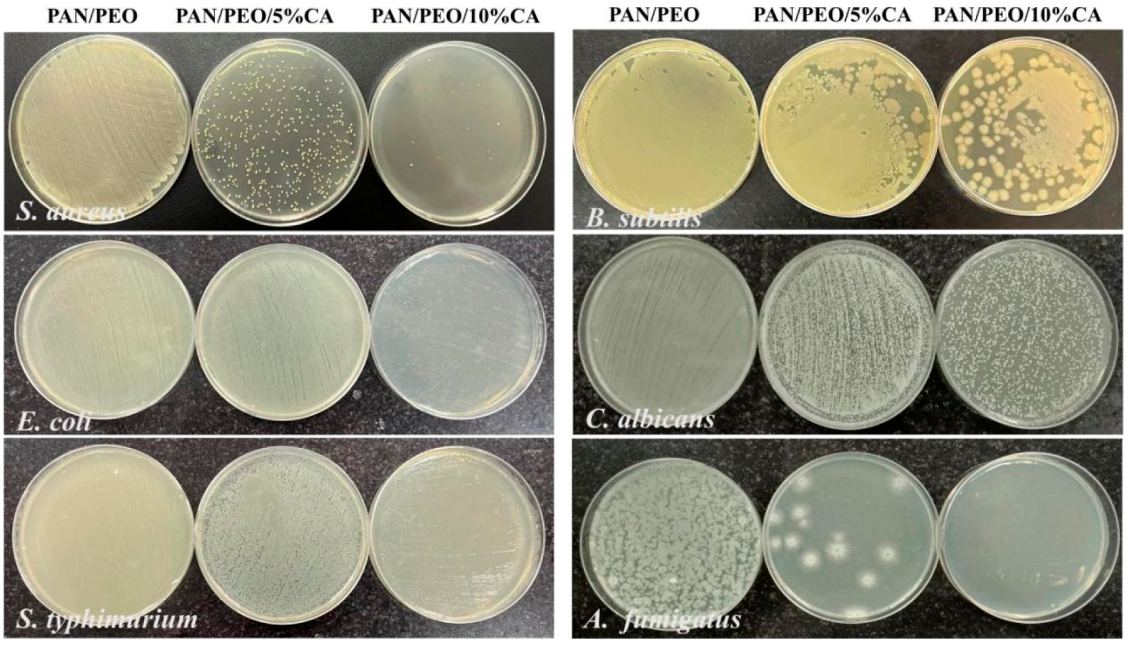

Figure 4. Microbial count observation following treatment with the PAN/PEO, PAN/PEO/5% CA, and PAN/PEO/10% CA nanofiber membranes.

3.3. Antimicrobial Performance Testing with the Diffusion Method. The antimicrobial efficiency of the CA-loaded PAN/PEO nanofibers was analyzed against Gram-negative bacteria (*E. coli* and *S. typhimurium*), Gram-positive bacteria (*S. aureus* and *B. subtilis*), and fungi (*C. albicans* and *A. fumigatus*). Diffusion experiments demonstrated that the PAN and PAN/PEO nanofiber membranes had nearly no antimicrobial effect. However, the PAN/PEO/5% CA and PAN/PEO/10% CA nanofiber membranes effectively inhibited the bacteria and fungi mentioned above (Figure 3). Compared with the PAN/PEO/5% CA nanofiber membrane, the PAN/PEO/10% CA nanofiber membrane exhibited significantly better antimicrobial effects.

3.4. Antimicrobial Performance Testing with the Oscillation Method. The different bacterial and fungal suspensions with the PAN/PEO, PAN/PEO/5% CA, and PAN/PEO/10% CA nanofiber membranes were incubated for 24 h, after which 100 μL of the bacterial suspension was evenly coated on the agar plate and incubated for another 24 h to obtain the results shown in Figure 4. The difference in microbe count reflected the antimicrobial effect of nanofiber membranes with different concentrations of CA. The number of colonies decreased with an increasing CA concentration, which suggested that the nanofiber membrane with CA exerted an antimicrobial effect, and the effect of PAN/PEO/CA with a relatively high concentration of CA was more pronounced. This result was consistent with the results of the drug sensitivity experiments shown in Figure 3, which further demonstrated the antimicrobial ability of the PAN/PEO/CA nanofiber membranes.

https://doi.org/10.1021/acsomega.4c03140
ACS Omega 2024, 9, 39472−39483

3.5. Effect of PAN/PEO/CA on *S. aureus* Morphology. SEM and TEM analyses were further conducted to confirm the impact of the PAN/PEO, PAN/PEO/5% CA, and PAN/PEO/10% CA nanofiber membranes on the number and morphology of *S. aureus*. The destructive effect of PAN/PEO/CA on *S. aureus* was intuitively illustrated in Figure 5A. *S. aureus* was aggregated and connected three-dimensionally in the PAN/PEO group, while the number of *S. aureus* decreased and *S. aureus* was scattered in the PAN/PEO/CA groups, which was in accordance with the results depicted in Figure 4.

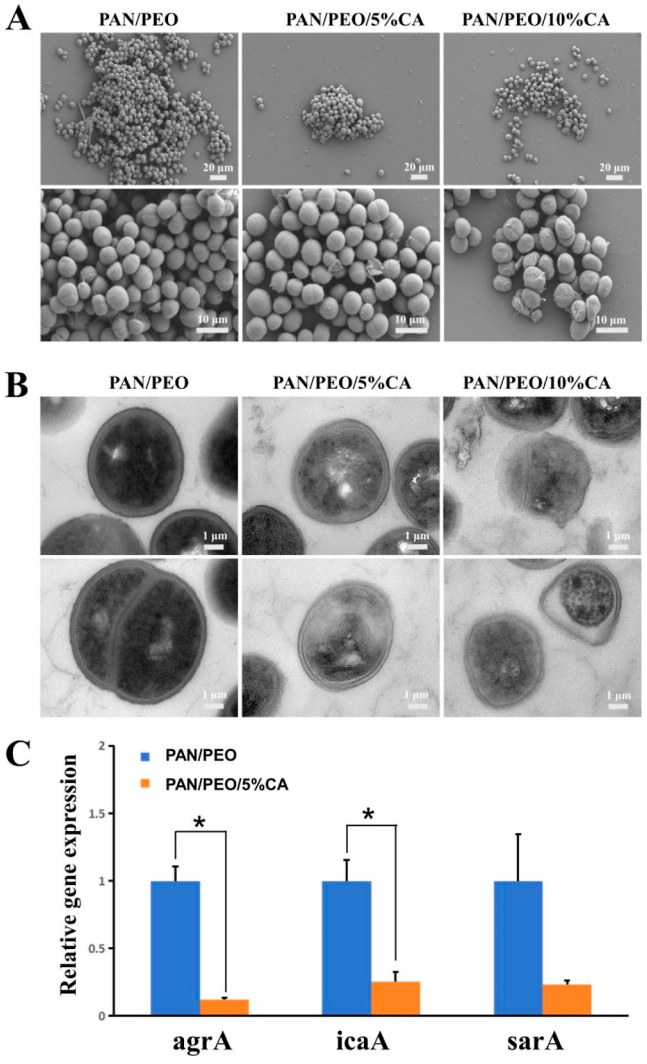

Figure 5. PAN/PEO/CA nanofiber membrane inhibits the formation of biofilms. SEM (A) and TEM (B) results of the PAN/PEO, PAN/PEO/5% CA, and PAN/PEO/10% CA nanofiber membranes. (C) Comparison of gene expression related to biofilm genes in *S. aureus* obtained by treatment with the PAN/PEO and PAN/PEO/5% CA nanofiber membranes. $^{*}p < 0.05$.

The ultrastructure of *S. aureus* was observed by TEM (Figure 5B). The *S. aureus* in the PAN/PEO group had a complete and clear bacterial cell structure with normal morphological characteristics and a uniform cytoplasmic region without the release of intracellular components. However, the edges of the cell wall and membrane become blurred, and the uniformity of the cytoplasm region was disturbed in the PAN/PEO/5% CA group. The cells in the PAN/PEO/10% CA group were seriously damaged. In addition to the loss of cellular integrity, some of the cytoplasmic contents leaked out of *S. aureus*. It can be seen that *S. aureus* underwent shrinkage and deformation with compromised integrity of the cell structure in the PAN/PEO/CA group, this phenomenon was more evident in the group treated with a high concentration of CA.

Subsequently, the differential expression levels of biofilm-associated genes were further determined by RT-PCR (Figure 5C). The expression of the biofilm-forming gene *icaA* was downregulated in PAN/PEO/5% CA-treated *S. aureus* compared to PAN/PEO-treated *S. aureus*. Compared with those in PAN/PEO-treated *S. aureus*, the expression of biofilm-forming regulators such as *agrA* and *sarA* in PAN/PEO/5% CA-treated *S. aureus* was downregulated. Based on the SEM and TEM results mentioned above, it can be inferred that the PAN/PEO/5% CA nanofiber membrane has an antibiofilm effect.

3.6. In Vivo *S. aureus*-Infected Wound Healing. The antibacterial and healing activity of the nanofiber membranes containing CA was evaluated in vivo, for which we created full-thickness skin wounds on the backs of rats infected with *S. aureus*. Wounds in the treatment group were covered with the synthesized PAN/PEO or PAN/PEO/5% CA nanofiber membranes, and medical sterile transparent dressings were used as the control group. As shown in Figure 6A, all groups of wounds exhibited varying degrees of purulent infection on day 2. The control group exhibited evident bacterial infection and purulence in wounds, whereas the PAN/PEO and PAN/PEO/5% CA groups displayed less degree of purulence. These results corresponded to the antibacterial effects of the PAN/PEO/CA nanofiber membranes shown in Figures 3 and 4. At 10 days postsurgery, the PAN/PEO and PAN/PEO/5% CA groups demonstrated better healing effects than control groups, in particular, those in the PAN/PEO/5% CA group almost completely healed. Wound healing was significantly promoted in the PAN/PEO/5% CA group from 4 to 10 days after surgery compared with the control and PAN/PEO groups (Figure 6B). These results implied that the PAN/PEO/5% CA nanofiber membrane exerts a beneficial effect by positively regulating the healing of wounds infected with *S. aureus*.

3.7. In Vivo *S. aureus*-Infected Wound Healing, H&E Staining, and Collagen Deposition. Wound healing is a comprehensive process encompassing four overlapping phases, namely, hemostasis, inflammation, proliferation, and wound remodeling with scar tissue formation.[33,34] To histologically assess the wound healing effect, H&E staining was performed. On day 10, re-epithelialization was complete in all three groups, and the skin tissues in all three groups were regenerated in the form of the basic structure of the epithelial and dermal layers (Figure 7A). The skin appendages were noted in the PAN/PEO/5% CA and PAN/PEO groups, while no obvious skin appendages were detected in the center of the wound tissue in the control group, indicating less complete healing. Compared with the PAN/PEO group, the PAN/PEO/5% CA group had a thicker epidermal layer. In addition, the dermal reticular layer in the PAN/PEO/5% CA group displayed a darker color than that in the other two groups, indicating that the healed tissue was closer to the surrounding undamaged tissue. These results demonstrated that the PAN/PEO/5% CA nanofiber could be an excellent candidate for antibacterial wound dressing.

During wound repair, collagen is synthesized by fibroblasts, which constitute the primary component of the extracellular

https://doi.org/10.1021/acsomega.4c03140
ACS Omega 2024, 9, 39472−39483

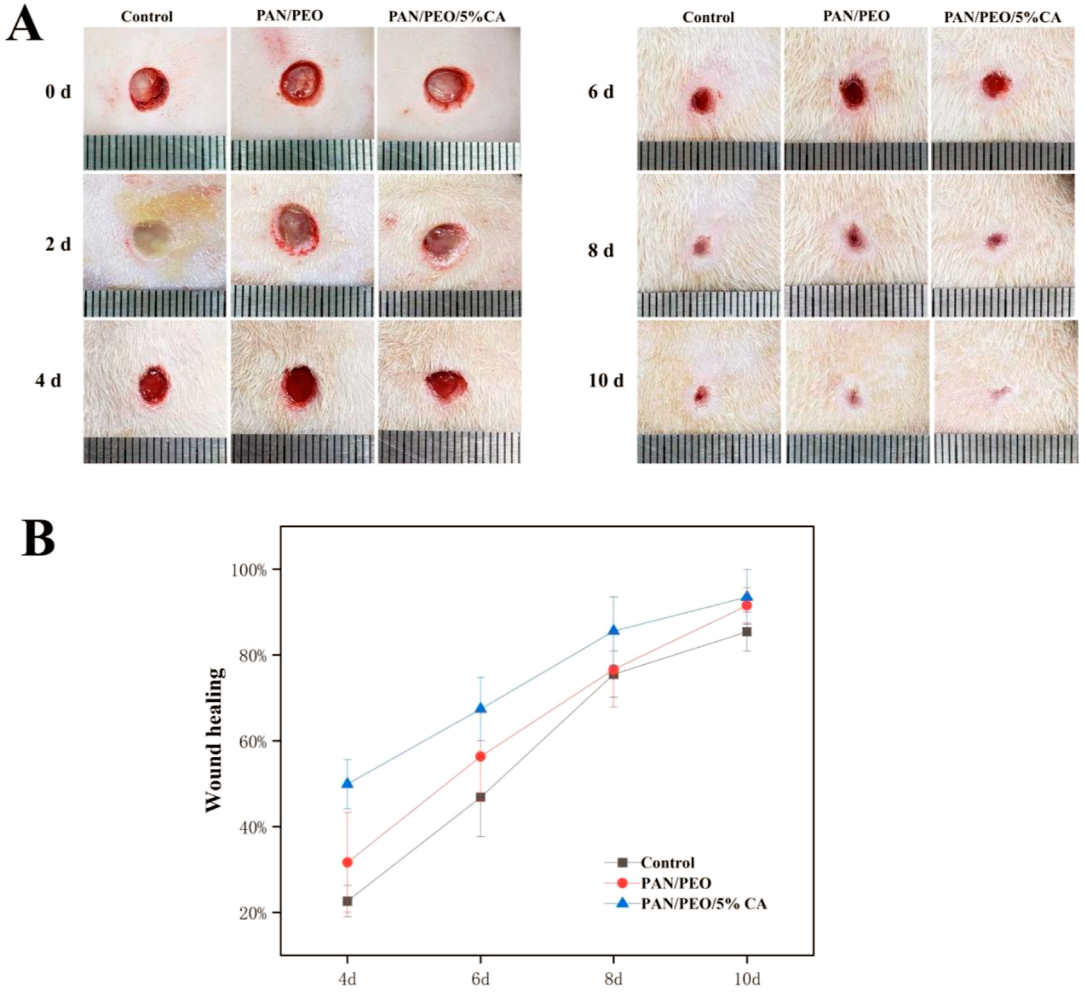

Figure 6. Wound healing process after infection. (A) Images of wound areas in the control, PAN/PEO, and PAN/PEO/5% CA groups at various time intervals. (B) Wound healing curves of control, PAN/PEO, and PAN/PEO/5% CA groups from days 4 to 10.

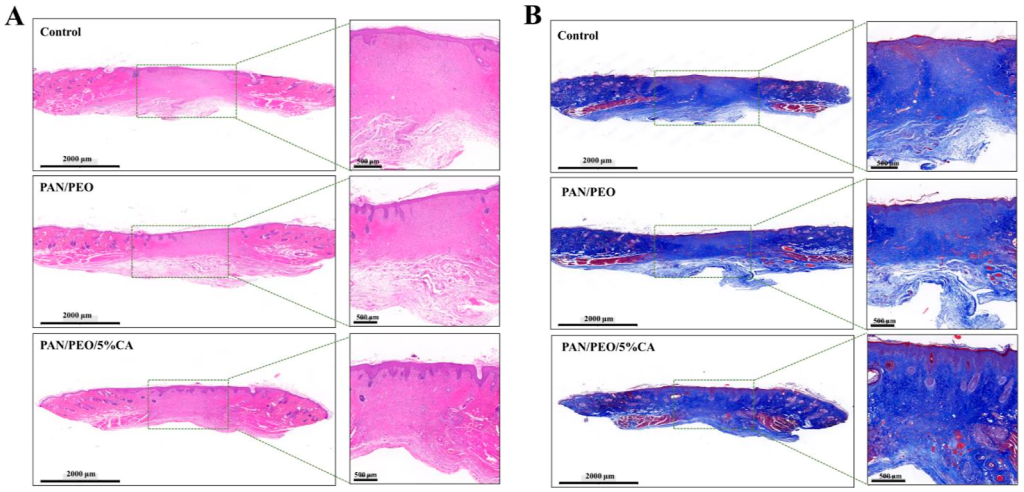

Figure 7. Histological images of *S. aureus*-infection wound tissue on day 10. (A) H&E staining. (B) Masson's trichrome staining.

matrix. The synthesis of collagen can effectively facilitate wound healing, and the degree of wound healing can be assessed by the amount of collagen deposited at the wound site.[35,36] Collagen deposition was evaluated through Masson's trichrome staining: blue indicates collagenous fiber, and red indicates muscle fibers. As shown in Figure 7B, the skin tissues displayed collagen deposition after healing for 10 days, and the color of the damaged healing area in the PAN/PEO/5% CA group was the darkest, whereas the color of the control group was the lightest, indicating that the group treated with PAN/PEO/5% CA had the greatest amount of collagen deposition. These results indicated that the *S. aureus*-infected skin wounds

https://doi.org/10.1021/acsomega.4c03140
ACS Omega 2024, 9, 39472−39483

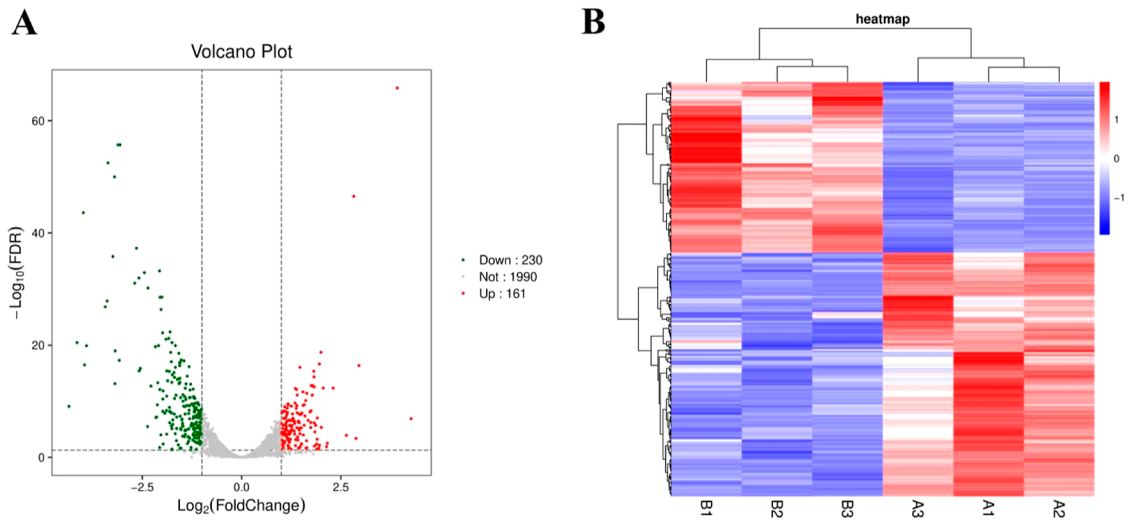

Figure 8. Transcriptomic analysis of *S. aureus* after PAN/PEO/5% CA and PAN/PEO treatment. (A) Differential expression was identified by $|\log_2$ (fold change)| > 1 and FDR < 0.05. Downregulated DEGs are labeled with a green circle, upregulated DEGs with a red circle, and unchanged genes with a gray circle. (B) Heatmap of the hierarchical clustering based on 391 DEGs. A1, A2, and A3 represent the three replicates of the PAN/PEO treatment group, while B1, B2, and B3 represent the three replicates of the PAN/PEO/5% CA treatment group. Red and blue indicate up- and downregulated DEGs, respectively.

in the PAN/PEO/5% CA group healed better than those in the other groups.

3.8. Transcriptomic Analysis Reveals Potential PAN/PEO/CA Nanofiber Membrane Regulation in *S. aureus*. *3.8.1. Identification of DEGs.* The objective was to study specific genes related to *S. aureus* infection and better understand the molecular mechanism of PAN/PEO/CA in the process of *S. aureus*-induced wound infection. The effect of PAN/PEO/CA on the gene expression of *S. aureus* was assessed at the transcriptome-wide scale. Total cellular RNA samples were extracted from the PAN/PEO/5% CA and PAN/PEO groups for RNA sequencing. According to the criteria of a $|\log_2$ (fold change)| value > 1 and FDR < 0.05, 391 genes were identified as DEGs. Between the PAN/PEO/5% CA and PAN/PEO groups, 161 genes were upregulated, and 230 genes were downregulated (Figure 8A). Of the DEGs, 2 upregulated genes and 15 significantly downregulated genes displayed a $|\log_2$ (fold change)| > 3. According to the gene ID and gene name of the NCBI database, 2 upregulated genes encoded hypothetical proteins and YhgE/Pip domain-containing proteins, whereas 15 downregulated genes encoded phage holin, 2 phage tail proteins, bicomponent gamma-hemolysin HlgAB subunit A, complement convertase inhibitor Ecb, alcohol dehydrogenase AdhP, TDT family transporters, glutamate synthase large subunits, CHAP domain-containing proteins, bicomponent gamma-hemolysin HlgCB subunit C, 2 hypothetical proteins, DoxX family proteins, complement convertase inhibitor Efb, and immunoglobulin-binding protein Sbi.

The DEG profile was examined under PAN/PEO/5% CA treatment conditions, for which DEGs with similar metabolic functions were clustered by hierarchical clustering analysis using FPKM values. Clustering analysis demonstrated that the DEG expression patterns of *S. aureus* were distinctly altered by PAN/PEO/5% CA treatment (Figure 8B).

3.8.2. GO Analysis, KEGG Analysis, and Hub Gene Screening. GO analyses were conducted to classify the functions of the DEGs identified by RNA sequencing. As shown in Figure 9A, metabolic process, cell, and catalytic activities were the largest subgroups enriched for upregulated DEGs in the BP, CC, and MF categories. Moreover, cellular process, cell, and catalytic activity were the largest subgroups enriched for the downregulated DEGs in terms of biological processes, cellular components, and molecular functions.

We further elucidated the functions of these DEGs and explored their enriched metabolic or signal transduction pathways. In addition, the DEGs were mapped to terms from the KEGG pathway database. Among the top 20 downregulated enriched KEGG pathways, the DEGs were significantly enriched for *S. aureus* infection, ABC transporters, and the two-component system (Figure 9B). Cytoscape was applied to calculate the 10 nodes of DEGs, which were the most highly expressed when the MCC method was used, as shown in Figure 9C. *rplA*, *rplS*, *rpsN*, *rpIL*, *rpsT*, *rpmH*, *rpsU*, *BTN44-RS12950*, *adhE*, and *gltB* were identified as hub genes.

4. DISCUSSION

S. aureus is a widely distributed Gram-positive bacterium that usually colonizes skin tissue and nasal mucosa. It is the main pathogen of hospital infections and can easily lead to local purulent infections of the skin and soft tissue. Therefore, it is essential to investigate antimicrobial materials to treat *S. aureus* infection. We developed and successfully evaluated a new PAN/PEO-based nanofiber scaffold loaded with CA (PAN/PEO/CA). Fabrication of CA-incorporated nanofibers did not change the orientation or morphology of the nanofiber membranes. The successful embedding of CA into the electrospinning nanofiber membrane was also confirmed through FTIR analysis. Compared with those with pure PAN, PAN/PEO exhibited significant hydrophilicity, which gradually decreased with increasing CA concentration. The hydrophilicity of the material enables the dressing to effectively remove the fluid from the wound, which is crucial in the design and development of a dressing. Hesperidin-loaded PAN/PEO nanofibers were fabricated and evaluated for wound dressing application and were found to promote skin regeneration more effectively than hesperidin-free nanofibers.[24] Therefore, PAN/

https://doi.org/10.1021/acsomega.4c03140
ACS Omega 2024, 9, 39472−39483

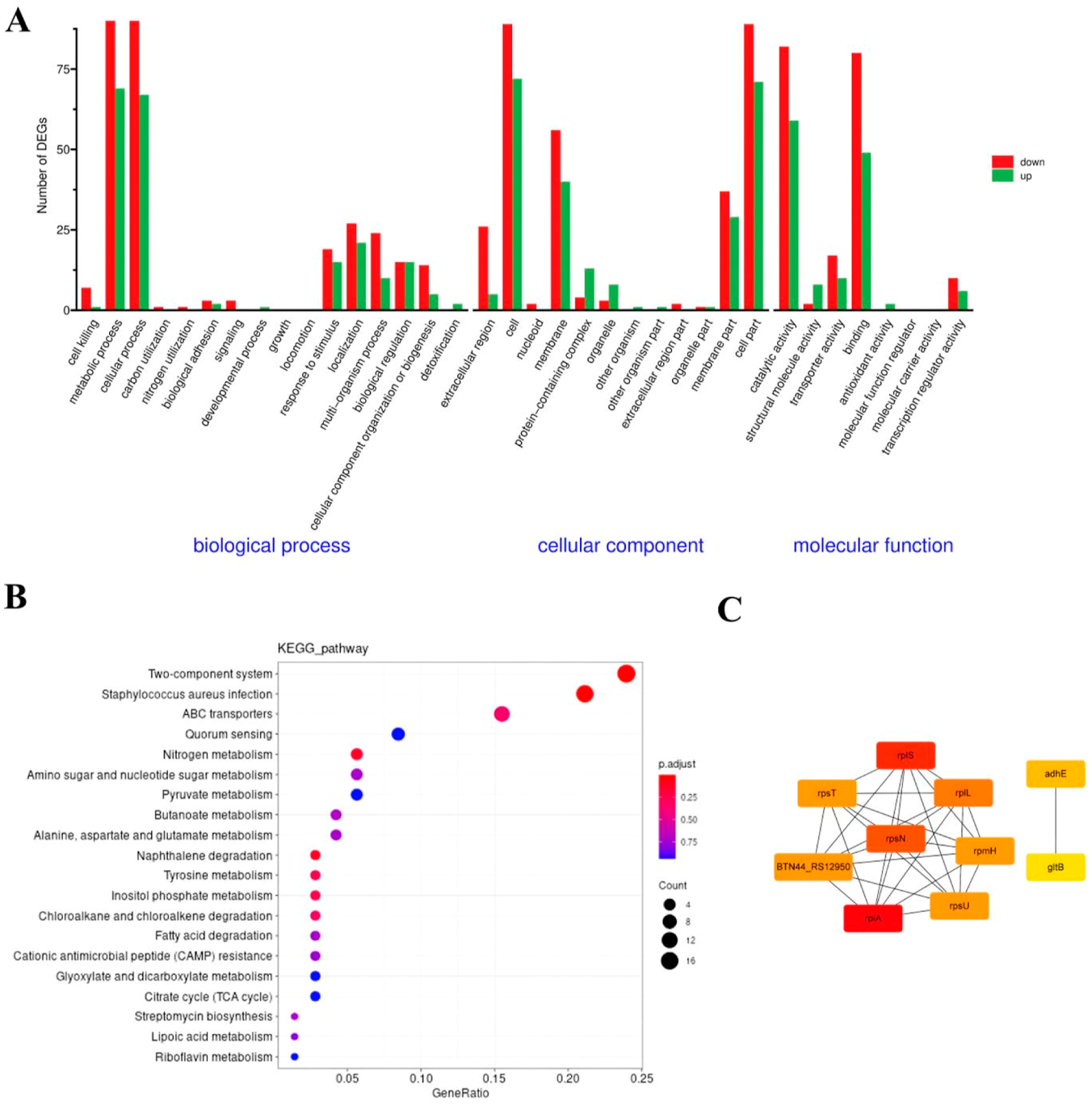

Figure 9. GO and KEGG analysis of *S. aureus* after PAN/PEO/5% CA and PAN/PEO treatment. (A) Histogram depiction of enriched GO classification of the DEGs. The *y*-axis indicates the gene numbers in each subcategory, and the top 10 subcategories in each main category are shown. (B) Functional analysis of DEGs based on the KEGG pathway. (C) The top 10 key genes were screened from 391 DEGs. The nodes represent genes, and the edges represent the links between the genes.

PEO nanofiber mats can be used as potential drug carriers to serve as wound dressings.

Diffusion and oscillation methods were used to evaluate the antimicrobial activity of the nanofiber membrane. Our results indicated that PAN/PEO/CA displayed antibacterial and antifungal activity against *S. aureus*, *E. coli*, *S. typhimurium*, *B. subtilis*, *C. albicans*, and *A. fumigatus*, and antimicrobial activity became stronger with increasing concentrations of CA when pure PAN nanofiber membranes and PAN/PEO nanofiber membranes displayed nearly no antimicrobial effect. The antimicrobial effects against Gram-negative and -positive bacteria and fungi were consistent with the literature.[37,38] CA has been extensively studied and shown to possess strong antibacterial properties against both Gram-positive and Gram-negative bacteria. Its mechanism of action involves several key pathways, including disruption of the bacterial membrane, inhibition of efflux pumps, and inhibition of membrane ATPases.[39] Studies investigating the antifungal effects of CA have demonstrated that its phenolic −OH group is essential for its activity. The hydrophobicity conferred by the aromatic ring enables CA to penetrate and damage membranes, resulting in high antifungal activity.[40]

https://doi.org/10.1021/acsomega.4c03140
ACS Omega 2024, 9, 39472−39483

The anti-*S. aureus* mechanism was studied by SEM, TEM, and RT-PCR. SEM and TEM micrographs revealed that CA disrupted the structural integrity of the cell wall. TEM revealed that *S. aureus* treated with the CA extract exhibited a shrunken cytoplasm and leakage of cell contents. Intercellular polysaccharide adhesins (polysaccharide intercellular adhesin, PIA) play a crucial role in the formation of biofilms. PIA is encoded by the *icaA* gene. Research has shown that the *icaA* gene is regulated by the *agrA* gene and *sarA* gene, and the expression levels of these genes are reduced to suppress biofilm formation in *S. aureus*.[41,42] The RT-PCR results demonstrated that the expression of biofilm-related genes (*icaA*, *agrA*, and *sarA*) decreased in the PAN/PEO/5% CA group compared to that in the PAN/PEO group. These findings suggest that PAN/PEO/CA has the potential for application as an antibacterial nanofiber membrane against *S. aureus* and inhibits the formation of *S. aureus* biofilms in vitro.

The antibacterial and prohealing effects of the PAN/PEO/5% CA nanofiber membranes were evaluated in a rat model of *S. aureus*-induced wound infection, and the PAN/PEO/5% CA group displayed less purulent infection on day 2, indicating that the PAN/PEO nanofibers loaded with CA can effectively inhibit the growth of *S. aureus*. On the other hand, the PAN/PEO nanofiber membrane also has the effect of adsorbing exudate. Comparing the time required for complete wound repair between the different groups, it was evident that the PAN/PEO/5% CA group exhibited the fastest and best repair results. To further confirm the repair effect of PAN/PEO/5% CA, H&E staining and Masson's trichrome staining were used to observe the generation of skin appendages and collagen, respectively. These findings explain the good repair effect of PAN/PEO/5% CA from a pathological perspective.

Infection was negatively associated with the healing status of wounds,[43] and skin infections in mice delayed the wound healing process compared to that in uninfected wounds.[44] *Lactobacillus johnsonii* and vitamin D supplementation could provide a valuable strategy for attenuating *S. aureus*-induced pathogenesis and promoting wound healing.[45] Similarly, we used a PAN/PEO nanofiber membrane with CA to reduce *S. aureus* infection and facilitate healing. Our RNA sequencing results revealed that compared with PAN/PEO, the PAN/PEO/5% CA nanofiber membrane downregulated the KEGG pathway enriched in the two-component system and *S. aureus* infection. These findings further indicate that the PAN/PEO/CA nanofiber membrane could promote the healing of skin wounds infected with *S. aureus*, providing a new strategy for the treatment of infected wounds.

5. CONCLUSIONS

In this research, a novel PAN/PEO/CA nanofiber membrane with antibacterial ability was successfully synthesized for promoting the wound healing of full-thickness skin infection with *S. aureus* via an electrospinning technique. It was demonstrated that the PAN/PEO/CA nanofiber membrane possessed a larger diameter and rougher surface. More serious damage to the biofilm structure was accompanied by a rise in antimicrobial activity with an increasing CA concentration in vitro. In an *S. aureus*-infected full-thickness skin wound healing model, the PAN/PEO/CA nanofiber membrane helped to kill bacteria and reduce purulent infection, promote re-epithelialization and subsequent deposition of collagen, and forming the structure of skin appendages such as hair follicle to accelerate the healing rate of wounds. The downregulated KEGG pathway analysis further revealed that the DEGs were significantly enriched in the two-component system and *S. aureus* infection. The PAN/PEO/CA nanofiber membrane showed effective antibacterial and wound-healing activity and can be used as a potential candidate material for wound healing. In future research, the ratio of PAN to PEO can be adjusted to detect their fiber morphology, porosity, and hydrophilicity, laying a foundation for better materials for dressings. Moreover, the antibacterial and skin wound recovery effects of using PAN/PEO as a carrier and loading other antibacterial components will be studied.

AUTHOR INFORMATION

Corresponding Author

Bei Xie − *Changde Hospital, Xiangya School of Medicine, Central South University (The First People's Hospital of Changde City), Changde 415000, China;* orcid.org/0009-0005-2755-936X; Email: xiaoningbeike@hnu.edu.cn

Authors

Shuo Wang − *Puai Medical School, Shaoyang University, Shaoyang 422000, China*

Xinyuan Xu − *Diagnostic Molecular Laboratory, Shaoyang University, Shaoyang 422000, China*

Xiangyu Zhu − *Diagnostic Molecular Laboratory, Shaoyang University, Shaoyang 422000, China*

Xiao Tan − *Diagnostic Molecular Laboratory, Shaoyang University, Shaoyang 422000, China*

Complete contact information is available at: https://pubs.acs.org/10.1021/acsomega.4c03140

Author Contributions

The manuscript was written through contributions of all authors. All authors have given approval to the final version of the manuscript.

Notes

The authors declare no competing financial interest.

ACKNOWLEDGMENTS

This work was supported by the Hunan Provincial Natural Science Foundation of China (2022JJ50211 and 2022JJ50204) and Research Project of Hunan Provincial Health Commission (B202304079292).

REFERENCES

(1) He, T.; Wang, J.; Huang, P.; Zeng, B.; Li, H.; Cao, Q.; Zhang, S.; Luo, Z.; Deng, D. Y.; Zhang, H.; Zhou, W. Electrospinning polyvinylidene fluoride fibrous membranes containing anti-bacterial drugs used as wound dressing. *Colloids Surf., B* **2015**, *130*, 278−286.

(2) Saeed, S. M.; Mirzadeh, H.; Zandi, M.; Barzin, J. Designing and fabrication of curcumin loaded PCL/PVA multi-layer nanofibrous electrospun structures as active wound dressing. *Prog. Biomater.* **2017**, *6* (1−2), 39−48.

(3) Chen, K.; Pan, H.; Ji, D.; Li, Y.; Duan, H.; Pan, W. Curcumin-loaded sandwich-like nanofibrous membrane prepared by electrospinning technology as wound dressing for accelerate wound healing. *Mater. Sci. Eng., C* **2021**, *127*, 112245.

(4) Alven, S.; Buyana, B.; Feketshane, Z.; Aderibigbe, B. A. Electrospun Nanofibers/Nanofibrous Scaffolds Loaded with Silver Nanoparticles as Effective Antibacterial Wound Dressing Materials. *Pharmaceutics* **2021**, *13* (7), 964.

(5) Eskandarinia, A.; Kefayat, A.; Agheb, M.; Rafienia, M.; Amini Baghbadorani, M.; Navid, S.; Ebrahimpour, K.; Khodabakhshi, D.; Ghahremani, F. A Novel Bilayer Wound Dressing Composed of a

https://doi.org/10.1021/acsomega.4c03140
ACS Omega 2024, 9, 39472−39483

Dense Polyurethane/Propolis Membrane and a Biodegradable Polycaprolactone/Gelatin Nanofibrous Scaffold. *Sci. Rep.* **2020**, *10* (1), 3063.
(6) Hadizadeh, M.; Naeimi, M.; Rafienia, M.; Karkhaneh, A. A bifunctional electrospun nanocomposite wound dressing containing surfactin and curcumin: In vitro and in vivo studies. *Mater. Sci. Eng., C* **2021**, *129*, 112362.
(7) Dodero, A.; Schlatter, G.; Hébraud, A.; Vicini, S.; Castellano, M. Polymer-free cyclodextrin and natural polymer-cyclodextrin electrospun nanofibers: A comprehensive review on current applications and future perspectives. *Carbohydr. Polym.* **2021**, *264*, 118042.
(8) Lanno, G. M.; Ramos, C.; Preem, L.; Putriņš, M.; Laidmäe, I.; Tenson, T.; Kogermann, K. Antibacterial Porous Electrospun Fibers as Skin Scaffolds for Wound Healing Applications. *ACS Omega* **2020**, *5* (46), 30011−30022.
(9) Chang, T.; Yin, H.; Yu, X.; Wang, L.; Fan, L.; Xin, J. H.; Yu, H. 3D PCL/collagen nanofibrous medical dressing for one-time treatment of diabetic foot ulcers. *Colloids Surf., B* **2022**, *214*, 112480.
(10) Huang, C.; Xu, X.; Fu, J.; Yu, D. G.; Liu, Y. Recent Progress in Electrospun Polyacrylonitrile Nanofiber-Based Wound Dressing. *Polymers* **2022**, *14* (16), 3266.
(11) Duan, H.; Chen, H.; Qi, C.; Lv, F.; Wang, J.; Liu, Y.; Liu, Z.; Liu, Y. A novel electrospun nanofiber system with PEGylated paclitaxel nanocrystals enhancing the transmucus permeability and in situ retention for an efficient cervicovaginal cancer therapy. *Int. J. Pharm.* **2024**, *650*, 123660.
(12) Serpelloni, S.; Williams, M. E.; Caserta, S.; Sharma, S.; Rahimi, M.; Taraballi, F. Electrospun Chitosan-Based Nanofibrous Coating for the Local and Sustained Release of Vancomycin. *ACS Omega* **2024**, *9* (10), 11701−11717.
(13) Huang, C.; Wang, M.; Yu, S.; Yu, D. G.; Bligh, S. W. A. Electrospun Fenoprofen/Polycaprolactone @ Tranexamic Acid/Hydroxyapatite Nanofibers as Orthopedic Hemostasis Dressings. *Nanomaterials* **2024**, *14* (7), 646.
(14) Zhao, P.; Zhou, K.; Xia, Y.; Qian, C.; Yu, D.-G.; Xie, Y.; Liao, Y. Electrospun trilayer eccentric Janus nanofibers for a combined treatment of periodontitis. *Adv. Fiber Mater.* **2024**, *6*, 1053−1073.
(15) Zhou, J.; Yi, T.; Zhang, Z.; Yu, D. G.; Liu, P.; Wang, L.; Zhu, Y. Electrospun Janus core (ethyl cellulose//polyethylene oxide) @ shell (hydroxypropyl methyl cellulose acetate succinate) hybrids for an enhanced colon-targeted prolonged drug absorbance. *Adv. Compos. Hybrid Mater.* **2023**, *6* (6), 189.
(16) Li, J.; Du, Q.; Wan, J.; Yu, D. G.; Tan, F.; Yang, X. Improved synergistic anticancer action of quercetin and tamoxifen citrate supported by an electrospun complex nanostructure. *Mater. Des.* **2024**, *238*, 112657.
(17) Zhong, W.; Xing, M. M.; Maibach, H. I. Nanofibrous materials for wound care. *Cutaneous Ocul. Toxicol.* **2010**, *29* (3), 143−152.
(18) Alotaibi, B. S.; Khan, A. K.; Kharaba, Z.; Yasin, H.; Yasmin, R.; Ijaz, M.; Khan, M.; Murtaza, G. Development of Poly(vinyl alcohol)-Chitosan Composite Nanofibers for Dual Drug Therapy of Wounds. *ACS Omega* **2024**, *9* (11), 12825−12834.
(19) Aker, S. D.; Tamburaci, S.; Tihminlioglu, F. Development of Cissus quadrangularis-Loaded POSS-Reinforced Chitosan-Based Bilayer Sponges for Wound Healing Applications: Drug Release and In Vitro Bioactivity. *ACS Omega* **2023**, *8* (22), 19674−19691.
(20) Canalli Bortolassi, A. C.; Guerra, V. G.; Aguiar, M. L.; Soussan, L.; Cornu, D.; Miele, P.; Bechelany, M. Composites Based on Nanoparticle and Pan Electrospun Nanofiber Membranes for Air Filtration and Bacterial Removal. *Nanomaterials* **2019**, *9* (12), 1740.
(21) Serag, E.; El-Aziz, A. M. A.; El-Maghraby, A.; Taha, N. A. Electrospun non-wovens potential wound dressing material based on polyacrylonitrile/chicken feathers keratin nanofiber. *Sci. Rep.* **2022**, *12* (1), 15460.
(22) Kupka, V.; Dvořáková, E.; Manakhov, A.; Michlíček, M.; Petruš, J.; Vojtová, L.; Zajíčková, L. Well-Blended PCL/PEO Electrospun Nanofibers with Functional Properties Enhanced by Plasma Processing. *Polymers* **2020**, *12* (6), 1403.
(23) Carvalho, L. D.; Peres, B. U.; Maezono, H.; Shen, Y.; Haapasalo, M.; Jackson, J.; Carvalho, R. M.; Manso, A. P. Doxycycline release and antibacterial activity from PMMA/PEO electrospun fiber mats. *J. Appl. Oral Sci.* **2019**, *27*, No. e20180663.
(24) Taymouri, S.; Hashemi, S.; Varshosaz, J.; Minaiyan, M.; Talebi, A. Fabrication and evaluation of hesperidin loaded polyacrylonitrile/polyethylene oxide nanofibers for wound dressing application. *J. Appl. Oral Sci.* **2021**, *32* (15), 1944−1965.
(25) Kim, C. H.; Khil, M. S.; Kim, H. Y.; Lee, H. U.; Jahng, K. Y. An improved hydrophilicity via electrospinning for enhanced cell attachment and proliferation. *J. Biomed. Mater. Res., Part B* **2006**, *78B* (2), 283−290.
(26) Singh, J.; Luqman, S.; Meena, A. Carvacrol as a Prospective Regulator of Cancer Targets/Signalling Pathways. *Curr. Mol. Pharmacol.* **2023**, *16* (5), 542−558.
(27) Scaffaro, R.; Maio, A.; Nostro, A. Poly(lactic acid)/carvacrol-based materials: preparation, physicochemical properties, and antimicrobial activity. *Appl. Microbiol. Biotechnol.* **2020**, *104* (5), 1823−1835.
(28) Celebioglu, A.; Yildiz, Z. I.; Uyar, T. Thymol/cyclodextrin inclusion complex nanofibrous webs: Enhanced water solubility, high thermal stability and antioxidant property of thymol. *Food Res. Int.* **2018**, *106*, 280−290.
(29) İnanç Horuz, T.; Belibağlı, K. B. Nanoencapsulation by electrospinning to improve stability and water solubility of carotenoids extracted from tomato peels. *Food Chem.* **2018**, *268*, 86−93.
(30) Hu, G.; Li, J.; Wang, Z.; Yang, W.; Hu, Y. PCL/Yam Polysaccharide nanofibrous membranes loaded with self-assembled HP-β-CD/ECG inclusion complexes for food packaging. *Food Chem.* **2024**, *438*, 138031.
(31) Fayemi, O. E.; Ekennia, A. C.; Katata-Seru, L.; Ebokaiwe, A. P.; Ijomone, O. M.; Onwudiwe, D. C.; Ebenso, E. E. Antimicrobial and Wound Healing Properties of Polyacrylonitrile-Moringa Extract Nanofibers. *ACS Omega* **2018**, *3* (5), 4791−4797.
(32) Fonseca, L. M.; Cruxen, C.; Bruni, G. P.; Fiorentini, Â. M.; Zavareze, E. D. R.; Lim, L. T.; Dias, A. R. G. Development of antimicrobial and antioxidant electrospun soluble potato starch nanofibers loaded with carvacrol. *Int. J. Biol. Macromol.* **2019**, *139*, 1182−1190.
(33) Guo, S.; Dipietro, L. A. Factors affecting wound healing. *J. Dent. Res.* **2010**, *89* (3), 219−229.
(34) Sorg, H.; Tilkorn, D. J.; Hager, S.; Hauser, J.; Mirastschijski, U. Skin Wound Healing: An Update on the Current Knowledge and Concepts. *Eur. Surg. Res.* **2017**, *58* (1−2), 81−94.
(35) Kallis, P. J.; Friedman, A. J. Collagen Powder in Wound Healing. *J. Drugs Dermatol.* **2018**, *17* (4), 403−408.
(36) Jung, H. S.; Kim, M. H.; Shin, J. Y.; Park, S. R.; Jung, J. Y.; Park, W. H. Electrospinning and wound healing activity of β-chitin extracted from cuttlefish bone. *Carbohydr. Polym.* **2018**, *193*, 205−211.
(37) Diao, M.; Yan, M.; Wang, Y.; Yan, X.; Dong, S.; Lu, Y.; Zhang, T. Characterization and antibacterial activity study of α-Lactalbumin-carvacrol complex. *Food Chem.* **2022**, *397*, 133820.
(38) Lazarevic, J. S.; Markovic, A.; Smelcerovic, A.; Stojanovic, G.; Ciuffreda, P.; Santaniello, E. Carvacrol Derivatives as Antifungal Agents: Synthesis, Antimicrobial Activity and in Silico Studies on Carvacryl Esters. *Acta Chim. Slov.* **2022**, *69* (3), 571−583.
(39) Kachur, K.; Suntres, Z. The antibacterial properties of phenolic isomers, carvacrol and thymol. *Crit. Rev. Food Sci. Nutr.* **2020**, *60* (18), 3042−3053.
(40) Konuk, H. B.; Ergüden, B. Phenolic -OH group is crucial for the antifungal activity of terpenoids via disruption of cell membrane integrity. *Folia Microbiol.* **2020**, *65* (4), 775−783.
(41) Kim, G. S.; Park, C. R.; Kim, J. E.; Kim, H. K.; Kim, B. S. Anti-Biofilm Effects of Torilis japonica Ethanol Extracts against Staphylococcus aureus. *J. Microbiol. Biotechnol.* **2022**, *32* (2), 220−227.
(42) Beenken, K. E.; Dunman, P. M.; McAleese, F.; Macapagal, D.; Murphy, E.; Projan, S. J.; Blevins, J. S.; Smeltzer, M. S. Global gene

https://doi.org/10.1021/acsomega.4c03140
ACS Omega 2024, 9, 39472−39483

expression in Staphylococcus aureus biofilms. *J. Bacteriol.* **2004**, *186* (14), 4665−4684.
(43) Fuentes, I.; Yubero, M. J.; Morandé, P.; Varela, C.; Oróstica, K.; Acevedo, F.; Rebolledo-Jaramillo, B.; Arancibia, E.; Porte, L.; Palisson, F. Longitudinal study of wound healing status and bacterial colonisation of Staphylococcus aureus and Corynebacterium diphtheriae in epidermolysis bullosa patients. *Int. Wound J.* **2023**, *20* (3), 774−783.
(44) Lecron, J.-C.; Charreau, S.; Jégou, J. F.; Salhi, N.; Petit-Paris, I.; Guignouard, E.; Burucoa, C.; Favot-Laforge, L.; Bodet, C.; Barra, A.; Huguier, V.; McHeik, J.; Dumoutier, L.; Garnier, J.; Bernard, F. X.; Ryffel, B.; Morel, F. IL-17 and IL-22 are pivotal cytokines to delay wound healing of S. aureus and P. aeruginosa infected skin. *Front. Immunol.* **2022**, *13*, 984016.
(45) Zanetta, P.; Ballacchino, C.; Squarzanti, D. F.; Amoruso, A.; Pane, M.; Azzimonti, B. Lactobacillus johnsonii LJO02 (DSM 33828) Cell-Free Supernatant and Vitamin D Improve Wound Healing and Reduce Interleukin-6 Production in Staphylococcus aureus-Infected Human Keratinocytes. *Pharmaceutics* **2024**, *16* (1), 18.

https://doi.org/10.1021/acsomega.4c03140
ACS Omega 2024, 9, 39472−39483